Ultrathin Gold–Shell Coated Silver Nanoparticles onto a Glass Platform for Improvement of Plasmonic Sensors

ARTICLE *in* ACS APPLIED MATERIALS & INTERFACES · MARCH 2013

Impact Factor: 6.72 · DOI: 10.1021/am4004254 · Source: PubMed

4 AUTHORS, INCLUDING:

Jiajia Deng
Nanyang Technological University
7 PUBLICATIONS **126** CITATIONS
SEE PROFILE

Junwei Di
Suzhou University
63 PUBLICATIONS **1,053** CITATIONS
SEE PROFILE

ACS APPLIED MATERIALS & INTERFACES

Research Article

www.acsami.org

Ultrathin Gold-Shell Coated Silver Nanoparticles onto a Glass Platform for Improvement of Plasmonic Sensors

Peipei Dong, Yuanyuan Lin, Jiajia Deng, and Junwei Di*

College of Chemistry, Chemical Engineering and Material Science, Key Lab of Health Chemistry and Molecular Diagnosis of Suzhou, Soochow University, Suzhou, Jiangsu 215123, People's Republic of China

Supporting Information

ABSTRACT: A facile and effective approach for the improvement of localized surface plasmon resonance (LSPR) biosensors based on silver-core and gold-shell nanoparticles (Ag@AuNPs) on a glass substrate was investigated. Silver nanoparticles (core) with thin gold shells on a transparent indium tin oxide (ITO) coated glass surface were prepared by sequential electrodeposition, and the influence of the thickness of the gold shell was systematically investigated. The experimental results indicate that the properties of an LSPR band of ultrathin (~1.3 nm) gold-shell coated silver nanoparticles are very similar to those of silver nanoparticles alone. The refractive index (RI) sensitivities of the metal nanostructures are calculated as 123 and 220 nm/RIU for the silver cores (~480 nm of LSPR peak) and Ag@AuNPs (~503 nm of LSPR peak), respectively, on the ITO substrate. The RI sensitivity of Ag@AuNPs was significantly enhanced by coating the silver nanoparticles with an ultrathin gold shell. This core–shell platform was also applied to the fabrication of biosensors. Thus, this strategy can be used to construct inexpensive, stable, versatile, and sensitive LSPR biosensors.

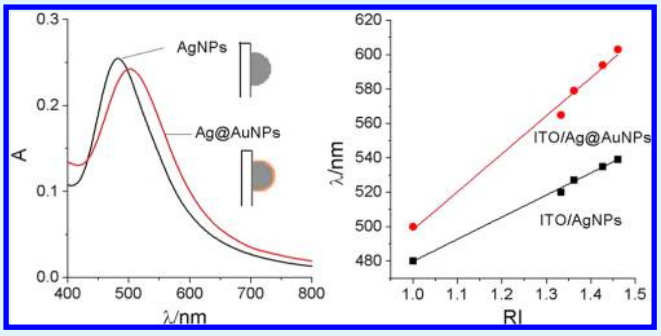

KEYWORDS: *silver core and gold shell, nanostructures, electrodeposition, plasmonic sensors*

1. INTRODUCTION

Localized surface plasmon resonance (LSPR) of noble-metal nanostructures has attracted much attention in recent years. The LSPR band is highly dependent on the composition, size, and shape of the nanoparticles, as well as on the refractive index (RI) of the dielectric medium around them.[1,2] The red-shift of LSPR induced by an increase in RI around the metal nanoparticles is the basis of LSPR sensing,[3−5] and directly monitoring the LSPR shifts of the nanoparticles upon binding of an analyte provides a direct and label-free method for bioassays.

A variety of metal nanoparticles in solution[6,7] or immobilized on solid surfaces[8−11] has been used for LSPR sensing. Using substrate-based nanostructures as platforms for chemical sensing is advantageous in several respects.[12,13] For example, metal nanoparticles supported on a solid substrate can provide not only good stability but also a consistent and stable sensor response to nanostructures. Moreover, the supported metal nanoparticles are free of organic stabilizers, making their surfaces readily accessible for functionalization with specific biomolecules. Transparent glass is the most popular supporting material for LSPR sensors. However, substrate-supported nanoparticles suffer an intrinsic drawback compared to nanoparticles in solution. The substrate supported metal nanoparticles are less sensitive to bulk changes than metal nanoparticles in a homogeneous environment because some of the electromagnetic field associated with LSPR is contained within the substrate.[14,15] For example, the RI sensitivity of small trigonal gold prisms deposited onto a clean glass substrate was only approximately half of that observed in bulk media.[16] Therefore, it is very useful to develop a simple strategy for reducing the substrate effect. Dmitriev et al.[17] reported that the effect of the substrates could be substantially reduced by supporting nanoplasmonic structures on dielectric pillars. Larsson et al.[18] prepared gold nanorings to enhance the RI sensitivity of LSPR sensors by reducing the contact area of the nanorings with the substrate more than that of similar nanodisks. In our previous paper,[19] we reported the fabrication of gold-core and silver-shell nanostructures as another candidate, in which the thin shells could significantly increase sensitivity by increasing the electric field of the core–shell interface.

The vast majority of LSPR sensing experiments have generally been performed using either gold nanoparticles (AuNPs) or silver nanoparticles (AgNPs) because they can exhibit LSPRs in the visible wavelength range. Gold is often chosen because of its chemical stability and resistance to oxidation. In contrast, AgNPs have sharper resonance, stronger absorbance,[20] and RI sensitivity,[21,22] which is more favorable in the application of LSPR sensors. For example, the extinction

Received: September 19, 2012
Accepted: March 11, 2013
Published: March 11, 2013

Scheme 1. Preparation of Ultrathin Gold Shell Coated AgNPs onto a Glass Platform for Biosensing

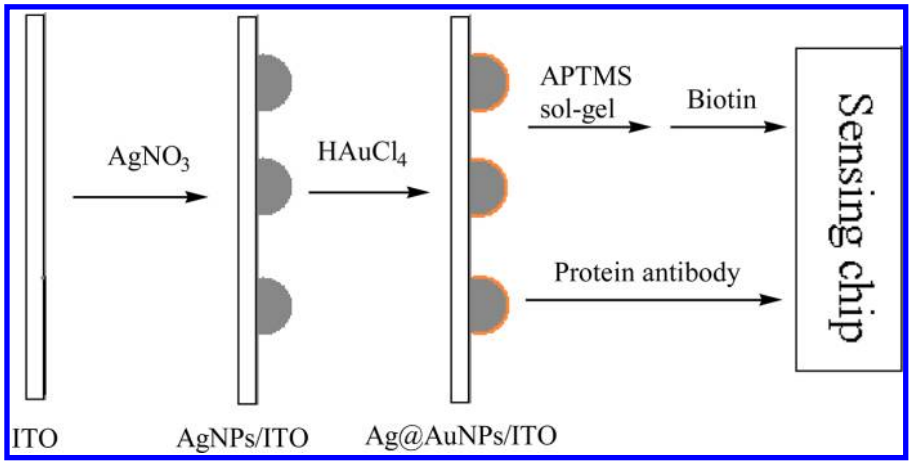

coefficient of the LSPR band for AgNPs is approximately four times larger than that for AuNPs of the same size.[20] A comparison of AuNPs and AgNPs of similar size and shape highlights this fact.[22−24] Coating AuNPs with a thin shell of silver can reduce the plasmon linewidth.[25] Moreover, the RI sensitivity of the gold-core and silver-shell nanostructures was found to be much greater than that of uncoated gold nanostructures that have a plasmon wavelength close to that of the core−shell nanostructures.[22,26] However, the toxicity of AgNPs hinders their use in bioapplications.[27] Additional thin films, such as silica[27] or gold,[28] were employed to cover the surface of AgNPs. Therefore, it is useful to think of a strategy that uses the advantages of both AgNPs and AuNPs to benefit the LSPR sensors.

Bimetallic core−shell nanoparticles are of great interest compared to monometallic nanoparticles. The LSPR signatures of these core−shell nanomaterials can be controlled not only by the core but also by the shell thickness.[29,30] Ultra high vacuum (UHV) deposition of silver and then of gold can lead to core−shell particles, but the synthesis might be sophisticated.[31−34] Synthesizing silver-core and gold-shell nanoparticles (Ag@AuNPs) with wet chemical methods remains challenging because of the significant etching of silver cores by $HAuCl_4$, a process known as galvanic replacement, which leads to nonuniform gold coatings and pinholes in the structure.[30] The use of electrochemical approach may help overcome this drawback. Herein, we demonstrate that ultrathin gold-shell coated AgNPs on a glass substrate can integrate the advantages of both the individual AuNPs and AgNPs. Moreover, the RI sensitivity of this proposed LSPR sensor is much higher than that of AuNPs or AgNPs on an indium tin oxide (ITO) substrate. The major contribution of this work is the integration of the advantages of AgNPs and AuNPs as well as a significant enhancement in the sensitivity. This approach provides new and useful strategies for developing excellent LSPR biosensors (Scheme 1). In this study, AgNPs were grown on a transparent ITO substrate. Thin gold shells were then deposited on the silver surfaces. The sensing chips could then be easily developed after functionalizing the surface.

2.. EXPERIMENTAL SECTION

2.1. Reagents and Materials. Tetrachloroauric acid ($HAuCl_4$) and silver nitrate ($AgNO_3$) were purchased from Guoyao Chemical Reagent Co, Ltd., China. 11-Mercaptoundecanoic acid (MUA) and (3-aminopropyl)trimethoxysilane (APTMS) were obtained from Sigma-Aldrich. Biotin, streptavidin (SA), human IgG (h-IgG), and goat anti-h-IgG were purchased from Beijing Bioss Biotechnology Co., Led., China. ITO glass (1.1 mm of thickness, less than 100 Ω) was obtained from Suzhou NSG Electronics Co., Ltd. (Suzhou, China). All other reagents were of analytical quality. Twice-distilled water was used throughout the experiments.

2.2. Electrodeposition of Ag@AuNPs onto ITO Substrate. Ag@AuNPs were prepared by successive electrodeposition. The ITO (0.6 × 3.0 cm^2) electrode was cleaned using NH_3−H_2O (1:20), ethanol, and distilled water for 10 min sequentially in an ultrasonic bath. The AgNP cores were electrodeposited onto the ITO electrodes from a 0.3 mol/L KNO_3 solution containing 0.3 mol/L $AgNO_3$ kept at 30 °C by applying a cyclic voltammogram (CV) in the potential range of −0.15 to −0.45 V at 0.05 V/s for 100 cycles. The slides were then rinsed with water prior to further modification. Then, the deposition of a thin gold shell onto the silver surface was performed by immersing the ITO/AgNPs electrodes in a solution containing 0.01 mmol/L $HAuCl_4$ + 0.1 mol/L phosphate buffer solution (PBS, pH 2.0) kept at 30 °C and running a CV between 0.0 V and −0.2 V for 100 cycles at a scan rate of 0.05 V/s. We defined this strip as ITO/Ag@AuNPs.

2.3. Surface Chemical Modification. The strips were modified with different biomolecules for biosensing, as shown in Scheme 1. In order to obtain amine functionality on the nanoparticle surface, the ITO/Ag@AuNPs strips were immersed in APTMS sol solution for 2 h. After rinsing with water, the strips were incubated in 0.2 mmol/L of biotin solution for 4 h. The strips were then left in SA solution for 4 h. Next, the strips were rinsed with water and air-dried at room temperature before absorption measurements.

Since the gold surface is already clean with no organic ligands, proteins can be directly adsorbed on it. Therefore, the ITO/Ag@AuNPs strips were left in 100 μg/mL of goat anti-h-IgG and PBS buffer solution (pH 7.4) for 12 h at 4 °C. Then, the strips were incubated in different concentrations of h-IgG and PBS buffer solution for another 3 h. After rinsing and drying the samples, the absorption spectra were recorded.

2.4. Apparatus and Measurements. Electrochemical deposition was carried out with a CHI 830B electrochemical workstation (CH Instruments Co., Shanghai, China). A conventional three-electrode system consisting of a platinum wire auxiliary electrode, saturated calomel reference electrode, and modified ITO electrode as the working electrode was used. Scanning electron microscopy (SEM) was performed using an S-4700 SEM (Hitachi, Japan). X-ray diffraction (XRD) was obtained using X'Pert-Pro MPD (Panalytical, Holland). The absorption spectra were measured with by a TU-2810 spectrophotometer (Beijing Purkinje General Instrument Co., Ltd.). All the absorption measurements were collected under ambient conditions.

3. RESULTS AND DISCUSSION

3.1. Deposition of Ag@AuNPs on ITO Substrate Surface. It is known that preparation of metal nanoparticles deposited onto to a solid substrate involves nucleation and particles growth.[35−39] Figure 1A shows cyclic voltammograms

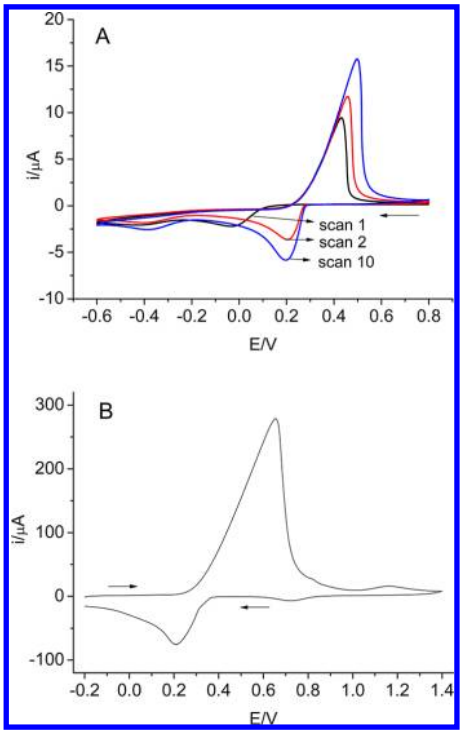

Figure 1. Cyclic voltammograms at 0.05 V/s for the deposition of silver from 0.3 mM $AgNO_3$ in 0.3 mM KNO_3 solution on ITO electrode surface (A) and for ITO/Ag@AgNPs electrode in 0.05 mol/L H_2SO_4 (B).

for $AgNO_3$ at the ITO electrode. The first scan contains a characteristic "nucleation loop" which results from the greater overpotential required for nucleation onto an ITO surface compared to that required for metals deposited on a metal surface.[36] The difference in the cathodic peak potential between the first scan and the subsequent scans is ∼0.2 V. The significant reduction in the overpotential required for deposition following the first scan indicates that subsequent growth occurs predominantly on the already-deposited metal sites rather than onto the bare ITO surface. Therefore, suitably chosen electrolytic conditions may favor one process over another, making it possible to tailor the number of deposited particles, as well as their particle size and distribution.

The AgNP cores were first synthesized from $AgNO_3$ using a silver source without any external reducing or stabilizing agents. The resultant AgNPs were then characterized by SEM images and UV-visible spectroscopy. The absorption peaks were located at ∼480 and ∼365 nm, corresponding to the excitation of dipolar and quadrupolar oscillations of AgNPs, respectively (Figure 2A).[40−42] It can be seen that the particles were well dispersed on the ITO surface. The average size of the prepared AgNPs was estimated to be 106 ± 12 nm (Figure 2B). Additionally, no free small AgNPs were observed in the SEM images. An atomic force microscopy (AFM) image was also recorded and analyzed to obtain more information about AgNPs (Figure S1, Supporting Information). The deposited AgNPs were quasi-hemispherical with height of ∼42 nm. Figure 3A shows the XRD pattern of AgNPs, which further demonstrates the formation of nanoparticles composed of pure silver. The overwhelmingly intensive diffraction peak was located at 2θ = 38.2°, which corresponds to the (111) lattice plane of silver.[43,44]

Ag@AuNPs were then fabricated by subsequent electrodeposition of gold onto the surface of the silver cores. In order to deposit an ultrathin film of gold, the applied potential needs to be precisely controlled. The potential range from 0 to −0.2 V was selected because gold has inchoative deposition and silver cannot be oxidized at this potential range (Figure S2, Supporting Information). This is an advantage of the use of electrodeposition rather than galvanic replacement. It is well known that the LSPR peak wavelength is highly dependent on both the shape and size of the nanoparticles, and the synthesis of a defined shape is very important for LSPR-based biosensors. Moreover, in the control experiment, no gold was electrodeposited on bare ITO surface at this potential range. Because a much larger overpotential is required for gold nucleation on a bare ITO surface, it is favorable for depositing gold on the sites of a silver nanocrystal due to the similar lattice constants of Ag and Au.[45,46] The XRD pattern of the resulting Ag@AuNPs was similar to that of AgNPs (Figure 3A). Therefore, by controlling the electrolysis potential, gold deposition occurs predominantly on the silver surface rather than on the bare ITO surface. The cyclic voltammogram (Figure 1B) and energy dispersive X-ray (EDX) spectrum of ITO/Ag@AuNPs (Figure 3B) demonstrated that gold was deposited on the sheet. Ag@AuNPs were formed because gold atoms can only bind to the preexisting silver particles. However, the formation of a Ag−Au alloy cannot be entirely excluded at the interface because of its roughness. The enlargement of the particles was caused by the deposition of the gold shell onto AgNP cores. The size of the nanoparticles increased with the increasing number of electrodeposition cycles, as shown in Figure 2C,D. The morphology of the nanoparticles was similar to that of AgNPs shown in Figure 2B. No small nanoparticles were observed on the substrate. The results of the SEM, XRD, and EDX analyses show that we cannot not rule out the possibility of defects on the ultrathin Au shell, especially in the first few deposition cycles. Nevertheless, the LSPR peaks of Ag@AgNPs were red-shifted with the increasing number of electrodeposition cycles (Figure 2A). Because the Au shell that formed after 20 cycles of electrodeposition on the Ag core was very thin, the shell thickness could not be determined directly from the SEM images (Figure 2B,C). Howover, the difference between AgNPs and Ag@AuNPs after 100 cycles of deposition could be measured from SEM images (Figures 2B,D). According to the relationship between Au-shell thickness and the number of cycles, the gold shell was estimated to be ∼1.3 nm thick after gold electrodeposition of 20 cycles. To confirm that the gold shell was very thin, we compared it with the SEM image of Ag@AuNPs by dissolving Ag in an aqueous $Fe(NO_3)_3$ solution (0.5 mol/L), which can be used as an etchant to dissolve Ag.[47] As shown in the Supporting Information (Figure S3), the nanostructures were fragmented into small pieces, which resulted from the ultrathin wall of the gold shell because it could not support itself.

Figure 2A displays the UV-vis absorption spectra of AgNPs and Ag@AuNPs as a function of various cycles of gold electrodeposition. After growing the gold shell on the silver core, the LSPR peak of Ag@AuNPs shifted to longer wavelengths and the relative intensity somewhat decreased

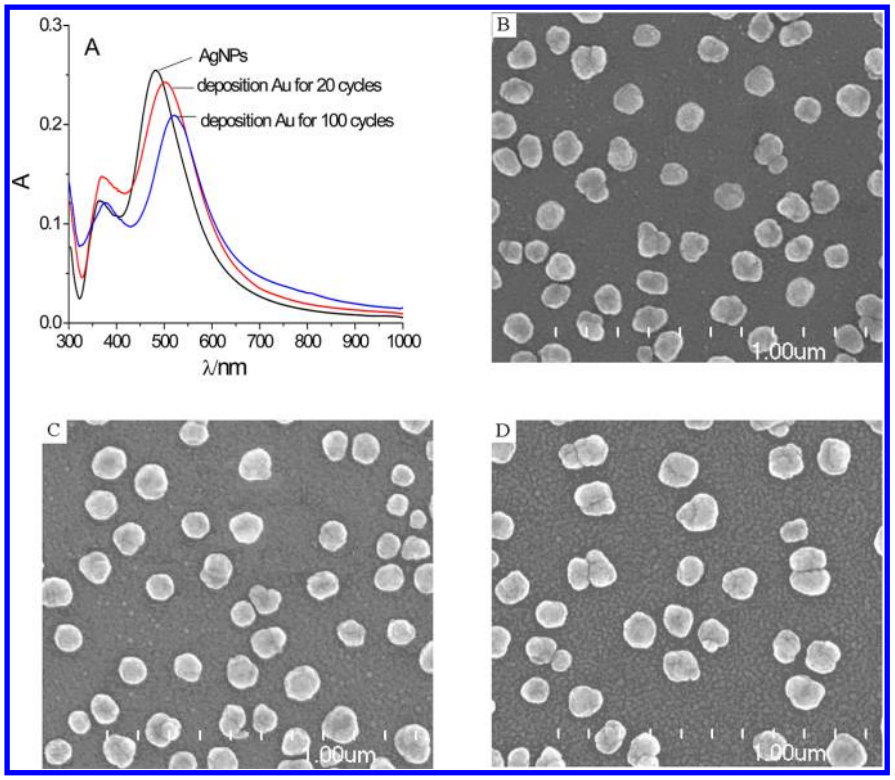

Figure 2. UV-vis absorption spectra of metal nanomaterials deposited on the surface of ITO substrate (A) and SEM image of Ag@AuNPs on ITO substrate (B) and then electrochemical deposition gold shell for 20 cycles (C) and 100 cycles (D).

with increasing gold-shell thickness. Moreover, after 100 cycles of gold deposition, a small shoulder located at ~540 nm appeared, which can be attributed either to a gold shell or to small spherical AuNPs on the ITO substrate. This phenomenon is in agreement with the experimental results of Hubenthal et al.[31] In fact, no small nanoparticles were observed on the ITO substrate in the SEM image. Therefore, from the UV-vis absorption spectra, we can reasonably infer that gold was deposited on the preformed silver-core surface rather than forming more nucleation sites, thus forming Ag@AuNPs. The UV-vis absorption spectra show a contribution from both the silver-core and the gold-shell plasmon absorptions. The red-shift of the LSPR peak could be caused by two factors. First, the dielectric constant of gold is different from that of silver, and thus, the dielectric constant varies with thickness of the gold coating. Second, homogeneous coating increases the diameter of the nanoparticle. These results indicate that the absorption peak of the Ag@Au nanoparticles is dominated by the core (Ag) and fine-tuned by the thin shell (gold). As the shell becomes thicker, Ag@AuNPs show behavior that is optically similar to that of pure AuNPs.

3.2. RI Sensitivity of ITO/Ag@AuNPs Platform. As the first test of the utility of Ag@AuNPs-modified ITO glass (ITO/Ag@AuNPs) as an LSPR sensor, we quantified the sensitivity of the strips in terms of changes in bulk RI. The UV-vis spectra of ITO/Ag@AuNPs in media with different refractive indices are shown in Figure 4. With increasing the RI, the LSPR peak was red-shifted for all samples. The peak wavelength of the LSPR was then plotted against the respective RI, and the sensitivity was obtained from the value of the slope per RI unit (RIU).

The thickness of the gold shells on the silver cores also significantly influences RI sensitivity. The ability to fine-tune and control the thickness of the gold shells allowed us to systematically study the effect of shell thickness on the RI sensitivity of the platform. The RI sensitivity of ITO/Ag@AuNPs rapidly increased with increasing number of electrodeposition cycles of gold shells (Figure 5). A plateau of sensitivity was obtained within 10−40 cycles of gold electrodeposition. With further increase in the number of deposition cycles, the RI sensitivity of ITO/Ag@AuNPs slowly decreased. The enhancement of RI sensitivity of the ITO/Ag@AuNPs platform could be attributed to an increase in the electric field for thin gold shell.[26,48] Wu et al.[48] studied the electric field enhancements in Ag@AuNPs in terms of the quasi-state theory. They found that the maximum enhancement occurs within a few nanometers of the shell surface, where the imaginary dielectric function values of the silver core and the gold shell are very different.[49] With increasing shell thickness, the contribution of the silver core was slowly reduced, accompanied by a gradual decrease in RI sensitivity. Therefore, 20 cycles was selected as the optimum for electrodeposition of gold shells on silver core surfaces. The RI sensitivity of ITO/Ag@AuNPs to the bulk RI was calculated to be ~220 nm/RIU, a 79% enhancement over the RI sensitivity of the ITO/AgNPs platform. This enhancement is similar to that of ITO/Au@AgNPs when compared to ITO/AuNPs.[19] These results indicate that the RI sensitivity of the LSPR sensor was significantly enhanced by depositing thin gold shells onto the silver surface of ITO/AgNPs. The RI sensitivity of 220 nm/RIU at 503 nm for ITO/Ag@AuNPs is very close to that of 252 nm/RIU at 700 nm for gold nanorods[50] and 245 nm/RIU at 705 nm for twin-linked AuNPs.[11]

In order to further confirm the effect of core−shell nanostructures, a different size of Ag@AuNPs was deposited on the ITO substrate surface using the same procedure. Figure S4, Supporting Information, shows the SEM images of AgNPs

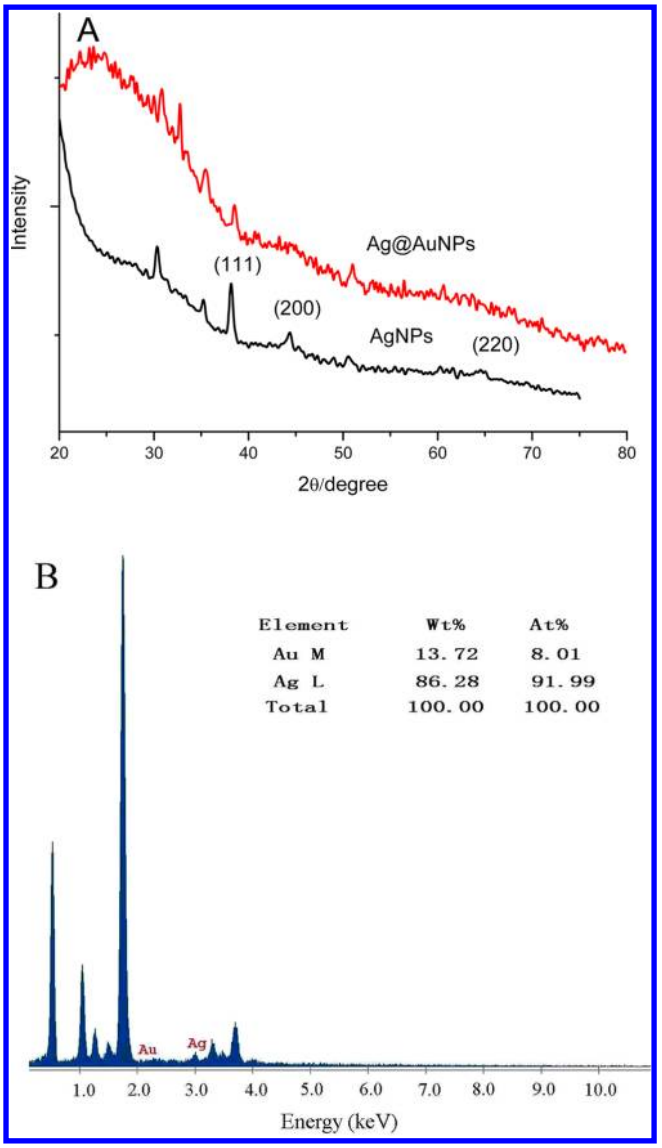

Figure 3. XRD patterns of metal nanoparticles (A) and EDX spectrum of Ag@AuNPs (B) deposited on ITO surface.

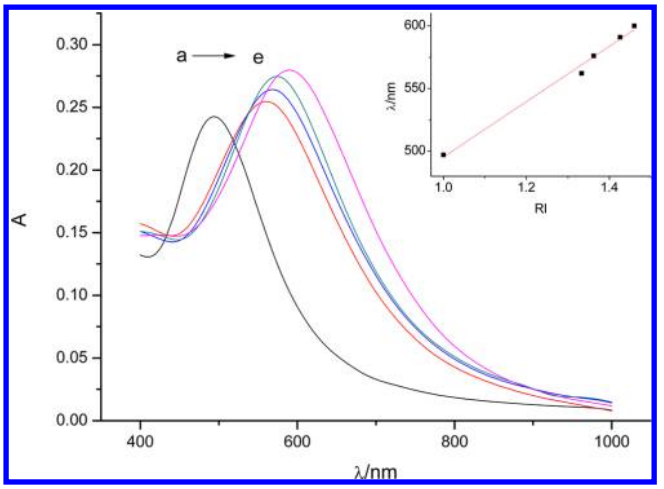

Figure 4. UV−vis absorption spectra of Ag@AuNPs deposited on ITO substrate in (a) air (n = 1.000), (b) water (n = 1.333), (c) ethanol (n = 1.362), (d) cyclohexane (n = 1.426), and (e) carbon tetrachloride (n = 1.461). Inset: Dependence of the LSPR peak shift on the refractive index for ITO/Ag@AuNPs.

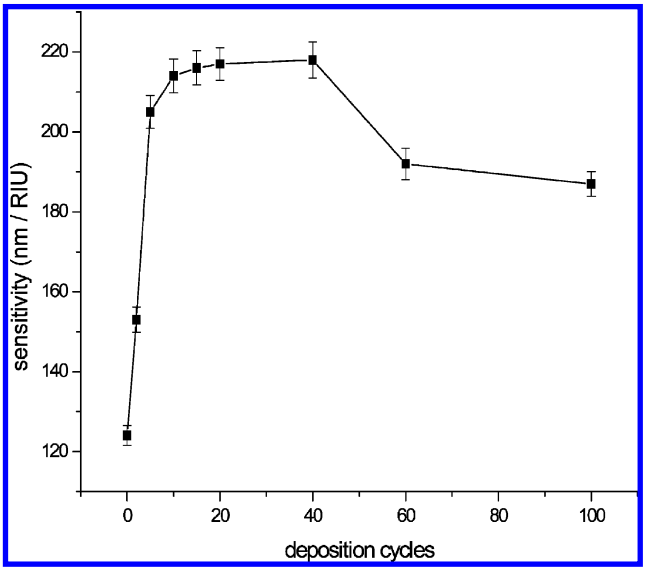

Figure 5. Relationship between the RI sensitivity and Au deposition cycles on ITO/AgNPs surface.

electrodeposited in the potential range of −0.3 to −0.6 V. The average size of AgNPs was 67 ± 8 nm. Next, thin gold shells were electrodeposited on the silver cores for 20 cycles. The resulting UV-vis absorption spectra are shown in Figure S5, Supporting Information. The LSPR peaks were located at ∼450 and ∼476 nm for AgNPs and Ag@AuNPs, respectively. Moreover, the RI sensitivities were investigated and calculated to be 81 and 143 nm/RIU for ITO/AgNPs and ITO/Ag@AuNPs, respectively. These results demonstrate that ultrathin gold shells covering silver cores onto a solid substrate could significantly enhance the RI sensitivity of AgNPs. It is known that the sensitivity of nanoparticles depends on the peak wavelength, shape, size, composition, and substrate. Miller and Lazarides[15] reported that the RI sensitivity of nanoparticles in solution followed a linear relationship with the peak wavelength and it decresed for nanoparticles assembled on a substrate. Chen et al.[51] demonstrated that the RI sensitivity was dependent on the shape of the metal nanoparticles for similar peak wavelengths, with large gold nanorods exhibiting the highest sensitivity and small nanorods exhibiting the lowest sensitivity. However, Morarescu et al.[52] observed that the sensitivity for small triangular AuNPs was higher than that for the large triangular nanoparticles. Up to now, it has remained difficult to answer precisely because the relationship between the sensitivity and nanoparticles is very complex.

3.3. LSPR Biosensors Based on ITO/Ag@AuNPs as a Platform. Molecular sensing using LSPRs can be illustrated by self-assembled monolayer (SAM) formation on the nanoparticle surface because SAMs of alkane thioles enable facile and well-known surface modification of AuNPs.[3] The sample strips were incubated in various MUA concentrations in ethanol for 2 h. After being cleaned and dried, the absorption spectra were recorded. The LSPR peak wavelength of ITO/Ag@AuNPs was red-shifted with increasing incubation concentration of MUA (Figure 6). The LSPR shifts showed observed a linear response to the presence of MUA in the range from 1×10^{-8} to 1×10^{-4} mol/L. This result is better than that reported for AgNP-based LSPR sensors.[8,53]

dx.doi.org/10.1021/am4004254 | ACS Appl. Mater. Interfaces 2013, 5, 2392−2399

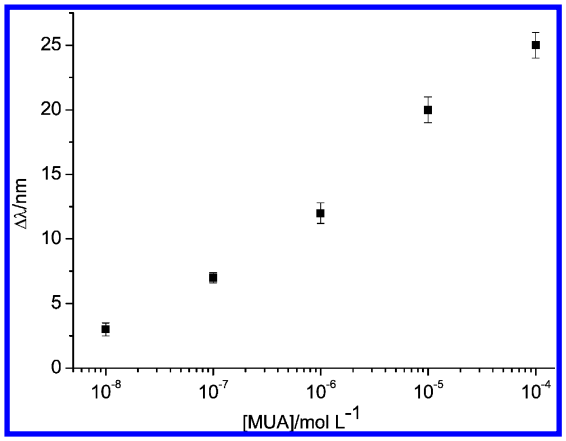

Figure 6. LSPR peak shift of the ITO/Ag@AuNPs with incubation at increasing MUA concentration.

An LSPR biosensor can be developed by the immobilization of biomolecules that target specific biologically relevant species on the gold surface from solution (Scheme 1). Biotin–SA was used as a model of a receptor–analyte system in order to investigate the LSPR sensor characterization. Biotin was immobilized on the gold surface using APTMS sol-gel which provides an amino-functionalized surface. The formation of a thin APTMS layer with a cross-linked silane polymer introduced a red-shift of ~5 nm (Figure 7A). The binding of biotin caused a further LSPR shift of ~4 nm. Finally, an additional red-shift of 11 nm was obtained after SA binding (1×10^{-8} mol/L). Figure 7B shows the response of the LSPR shift as a function of the concentration of SA. The red-shift of the LSPR peak linearly increased with increasing SA concentration in the range of 1×10^{-12} to 1×10^{-8} mol/L.

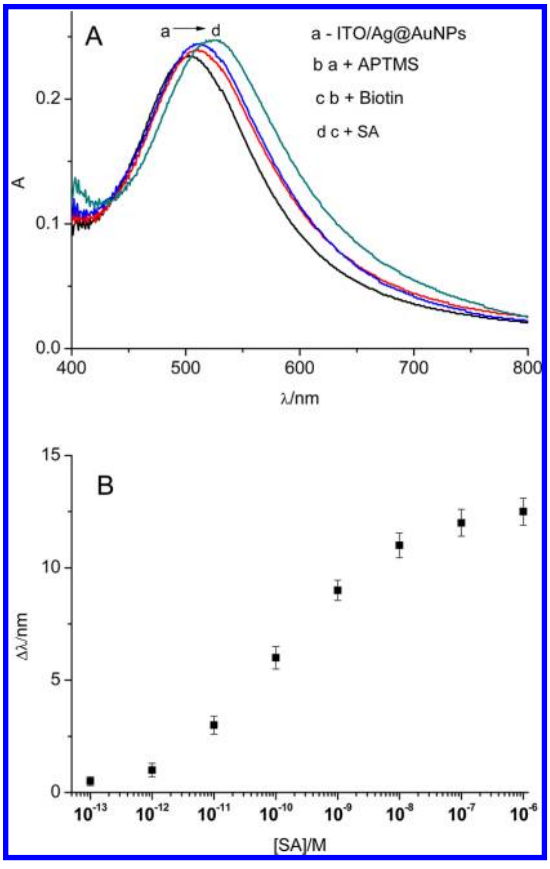

Figure 7. Monitoring the biotin–SA binding: LSPR spectra of ITO/Ag@AuNPs and after being incubated sequentially in AMTPS, biotin, and 1 μM SA (A). Relationship between the LSPR peak wavelength and the SA concentration (B).

To further examine the biosensing ability of ITO/Ag@AuNPs as a platform, a goat anti-h-IgG/h-IgG pair was employed as a model of a receptor–analyte system (Scheme 1). After incubation of the ITO/Ag@AuNPs strips with 100 μg/mL of anti-h-IgG in the PBS solution (pH 7.4) for 12 h at 4 °C, a 25 nm LSPR red-shift was observed. In the control experiments, no marked changes were observed in the absorption spectra before or after incubation of the strip in the buffer solution. When exposing the strips to different concentrations of h-IgG solution, the interaction of anti-h-IgG and h-IgG yielded a further LSPR red-shift (Figure 8A). Figure 8B shows the resulting calibration curve. The detection limit of h-IgG was 1 ng/mL. This result is similar to that reported for an LSPR biosensor based on gold nanorods.[9] In addition, the LSPR peak of the functionalized strip was red-shifted less than 1 nm after the incubation of 1 μg/mL mouse IgG solution in the control experiments, which suggested good specificity of the biosensor. These results clearly indicate the potential of Ag@AuNPs for biosensor applications.

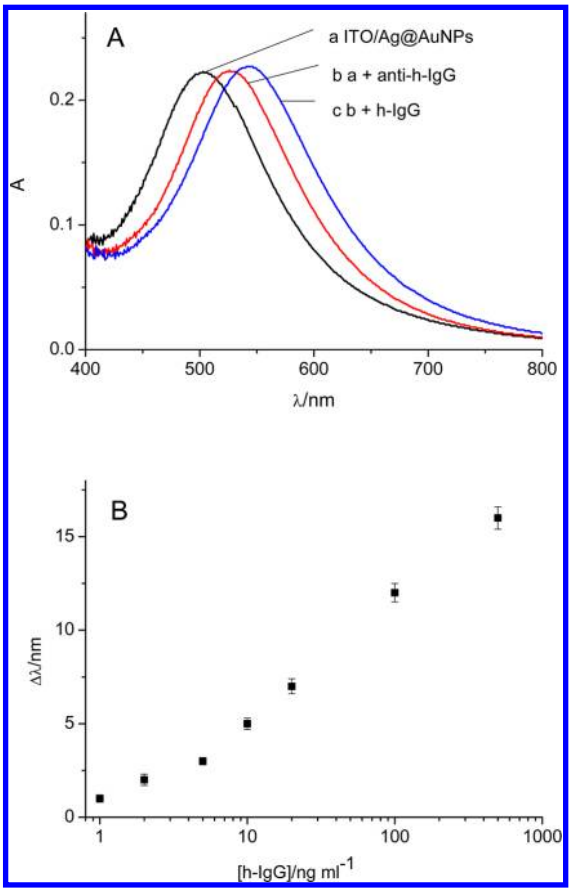

Figure 8. Monitoring the antibody–antigen binding: LSPR spectra of ITO/Ag@AuNPs, after being incubated in goat anti-h-IgG and after binding of 500 ng/mL h-IgG (A). Calibration curve for detection of h-IgG in solution at different concentrations (B).

4. CONCLUSIONS

In this work, we demonstrated that an ultrathin gold shell deposited on a silver core on a glass substrate is a good method for improving the performance of LSPR sensors. The method described in this paper has several significant benefits: (1) The RI sensitivity of this nanostructure is significantly enhanced as compared to AgNP-based LSPR sensors; (2) the gold shell on the silver core provides better chemical stability and less toxicity than AgNPs; (3) the plasmon absorption band of the core−shell nanostructures is similar to that of silver cores, which is favorable for application in LSPR sensors due to its sharp shape, strong absorbance, and high RI sensitivity; (4) the relative low peak wavelength compared to that of similar sized AuNPs would be a benefit for the development of a more sensitive LSPR sensor in the visible spectral range. Therefore, the LSPR-sensing improvement strategy presented in this paper can significantly benefit further development of nanoplasmonic-based optical biosensors.

■ ASSOCIATED CONTENT

Supporting Information

AFM images and height profile of AgNPs deposited on ITO substrate; cyclic voltammograms for the deposition of gold on an ITO electrode; SEM images of Ag@AuNPs after treatment with 0.5 mol/L of $Fe(NO_3)_3$ and its cyclic voltammogram in H_2SO_4 solution; SEM image of AgNPs deposited in the potential range of −0.3 to −0.6 V and UV-vis absorption spectra of AgNPs and Ag@AuNPs. This material is available free of charge via the Internet at http://pubs.acs.org.

■ AUTHOR INFORMATION

Corresponding Author

*E-mail: djw@suda.edu.cn.

Notes

The authors declare no competing financial interest.

■ ACKNOWLEDGMENTS

This work was financially supported by the National Natural Science Foundation of China (No. 21075086), the Project of Scientific and Technologic Infrastructure of Suzhou (SZS201207), and the Priority Academic Program Development of Jiangsu Higher Education Institutions.

■ REFERENCES

(1) Cortie, M. B.; McDonagh, A. M. *Chem. Rev.* **2011**, *111*, 3713−3735.
(2) Kelly, K. L.; Coronado, E.; Zhao, L. L.; Schatz, G. C. *J. Phys. Chem. B* **2003**, *107*, 668−677.
(3) Mayer, K. M.; Hafner, J. H. *Chem. Rev.* **2011**, *111*, 3828−3857.
(4) Sepúlveda, B.; Angelomé, P. C.; Lechuga, L. M.; Liz-Marzán, L. M. *Nano Today* **2009**, *4*, 244−251.
(5) Haes, A. J.; Van Duyne, R. P. *Anal. Bioanal. Chem.* **2004**, *379*, 920−930.
(6) Sun, Y.; Xia, Y. *Anal. Chem.* **2002**, *74*, 5297−5305.
(7) Li, C.; Wu, C.; Zheng, J.; Lai, J.; Zhang, C.; Zhao, Y. *Langmuir* **2010**, *26*, 9130−9135.
(8) Fan, M.; Thompson, M.; Andrade, M. L.; Brolo, A. G. *Anal. Chem.* **2010**, *82*, 6350−6352.
(9) Wang, C.; Ma, Z.; Wang, T.; Su, Z. *Adv. Funct. Mater.* **2006**, *16*, 1673−1678.
(10) Zhu, S.; Du, C.; Fu, Y. *Opt. Mater.* **2009**, *31*, 1608−1613.
(11) Deng, J.; Song, Y.; Wang, Y.; Di, J. *Biosens. Bioelectron.* **2010**, *26*, 615−619.
(12) Stewart, M. E.; Anderton, C. R.; Thompson, L. B.; Maria, J.; Gray, S. K.; Rogers, J. A.; Nuzzo, R. G. *Chem. Rev.* **2008**, *108*, 494−521.
(13) Rashid, M. H.; Bhattacharjee, R. R.; Mandal, T. K. *J. Phys. Chem. C* **2007**, *111*, 9684−9693.
(14) Malinsky, M. D.; Kelly, K. L.; Schatz, G. C.; Van Duyne, R. P. *J. Phys. Chem. B* **2001**, *105*, 2343−2350.
(15) Miller, M. M.; Lazarides, A. A. *J. Phys. Chem. B* **2005**, *109*, 21556−21565.
(16) Novo, C.; Funston, A. M.; Pastoriza-Santos, I.; Liz-Marzán, L. M.; Mulvaney, P. *J. Phys. Chem. C* **2008**, *112*, 3−7.
(17) Dmitriev, A.; Hägglund, C.; Chen, S.; Fredriksson, H.; Pakizeh, T.; Käll, M.; Sutherland, D. S. *Nano Lett.* **2008**, *8*, 3893−3898.
(18) Larsson, E. M.; Alegret, J.; Käll, M.; Sutherland, D. S. *Nano Lett.* **2007**, *7*, 1256−1263.
(19) Deng, J.; Du, J.; Wang, Y.; Tu, Y.; Di, J. *Electrochem. Commun.* **2011**, *13*, 1517−1520.
(20) Link, S.; Wang, Z. L.; El-Sayed, M. A. *J. Phys. Chem. B* **1999**, *103*, 3529−3533.
(21) Jakab, A.; Rosman, C.; Khalavka, Y.; Becker, J.; Trügler, A.; Hohenester, U.; Sönnichsen, C. *ACS Nano* **2011**, *5*, 6880−6885.
(22) Lee, Y.H.; Chen, H.; Xu, Q.; Wang, J. *J. Phys. Chem. C* **2011**, *115*, 7997−8004.
(23) Sekhon, J. S.; Verma, S. S. *Plasmonics* **2011**, *6*, 311−317.
(24) Lismont, M.; Dreesen, L. *Mater. Sci. Eng. C* **2012**, *32*, 1437−1442.
(25) Becker, J.; Zins, I.; Jakab, A.; Khalavka, Y.; Schubert, O.; Sönnichsen, C. *Nano Lett.* **2008**, *8*, 1719−1723.
(26) Steinbrück, A.; Stranik, O.; Csaki, A.; Fritzsche, W. *Anal. Bioanal. Chem.* **2011**, *401*, 1241−1249.
(27) Sotiriou, G. A.; Sannomiya, T.; Teleki, A.; Krumeich, F.; Vörös, J.; Pratsinis, S. E. *Adv. Funct. Mater.* **2010**, *20*, 4250−4257.
(28) Ehler, T. T.; Noe, L. J. *Langmuir* **1995**, *11*, 4177−4179.
(29) Jiang, R.; Chen, H.; Shao, L.; Li, Q.; Wang, J. *Adv. Mater.* **2012**, DOI: 10.1002/adma.201201896.
(30) Shahjamali, M. M.; Bosman, M.; Cao, S.; Huang, X.; Saadat, S.; Martinsson, E.; Aili, D.; Tay, Y.; Liedberg, B.; Loo, S. C. J.; Zhang, H.; Boey, F.; Xue, C. *Adv. Funct. Mater.* **2012**, *22*, 849−854.
(31) Hubenthal, F.; Borg, N.; Träger, F. *Appl. Phys. B* **2008**, *93*, 39−45.
(32) Benten, W.; Nilius, N.; Ernst, N.; Freund, H.-J. *Phys. Rev. B* **2005**, *72*, 045403.
(33) Hubenthala, F.; Ziegler, T.; Hendrich, C.; Alschinger, M.; Träger, F. *Eur. Phys. J. D* **2005**, *34*, 165−168.
(34) Sancho-Parramon, J.; Janicki, V.; Lončarić, M.; Zorc, H.; Dubček, P.; Bernstorff, S. *Appl. Phys. A* **2011**, *103*, 745−748.
(35) El Roustom, B.; Fóti, G.; Comninellis, C. *Electrochem. Commun.* **2005**, *7*, 398−405.
(36) Sheridan, E.; Hjelm, J.; Forster, R. J. *J. Electroanal. Chem.* **2007**, *608*, 1−7.
(37) Sandmann, G.; Dietz, H.; Plieth, W. *J. Electroanal. Chem.* **2000**, *491*, 78−86.
(38) Dávila-Martínez, R. E.; Cueto, L. F.; Sánchez, E. M. *Surf. Sci.* **2006**, *600*, 3427−3435.
(39) Hu, Y.; Song, Y.; Wang, Y.; Di, J. *Thin Solid Films* **2011**, *519*, 6605−6609.
(40) Kreibig, U.; Schmitz, B.; Breuer, H. D. *Phys. Rev. B* **1987**, *36*, 5027−5030.
(41) Upender, G.; Satyavathi, R.; Raju, B.; Shadak Alee, K.; Narayana Rao, D.; Bansal, C. *Chem. Phys. Lett.* **2011**, *511*, 309−314.
(42) Choi, Y.; Hong, S.; Liu, L.; Kim, S. K.; Park, S. *Langmuir* **2012**, *28*, 6670−6676.
(43) Hong, G.; Li, C.; Qi, L. *Adv. Funct. Mater.* **2010**, *20*, 3774−3783.
(44) Wani, I. A.; Khatoon, S.; Ganguly, A.; Ahmedb, J.; Ganguli, A.K.; Ahmad, T. *Mater. Res. Bull.* **2010**, *45*, 1033−1038.
(45) Ma, Y.; Li, W.; Cho, E. C.; Li, Z.; Yu, T.; Zeng, J.; Xie, Z.; Xia, Y. *ACS Nano* **2010**, *4*, 6725−6734.
(46) Park, G.; Seo, D.; Jung, J.; Ryu, S.; Song, H. *J. Phys. Chem. C* **2011**, *115*, 9417−9423.

(47) Lu, X.; Au, L.; McLellan, J.; Li, Z.; Marquez, M.; Xia, Y. *Nano Lett.* **2007**, *7*, 1764−1769.
(48) Wu, D.; Xu, X.; Liu, X. *Solid State Commun.* **2008**, *148*, 163−167.
(49) Bruzzone, S.; Malvaldi, M.; Arrighini, G. P.; Guidotti, C. *J. Phys. Chem. B* **2006**, *110*, 11050−11054.
(50) Marinakos, S. M.; Chen, S.; Chilkoti, A. *Anal. Chem.* **2007**, *79*, 5278−5283.
(51) Chen, H.; Shao, L.; Woo, K. C.; Ming, T.; Lin, H.; Wang, J. *J. Phys. Chem. C* **2009**, *113*, 17691−17697.
(52) Morarescu, R.; Träger, F.; Hubenthal, F. *Int. J. Circ. Syst. Signal Pr.* **2011**, *5*, 407−414.
(53) Barbillon, G.; Bijeon, J. L.; Plain, J.; de la Chapelle, M. L.; Adam, P.-M.; Royer, P. *Surf. Sci.* **2007**, *601*, 5057−5061.